doi.org/10.15407/tpwj2017.10.04

MODELING THERMOMECHANICAL PROCESSES IN WELDING HIGH-TECH PLASTICS WITH EMBEDDED ELEMENT*

R.V. KOLESNIK, M.V. YURZHENKO, N.G. KORAB, A.A. SHADRIN and **Yu.V. LITVINENKO**
E.O. Paton Electric Welding Institute of the NAS of Ukraine
11 Kazimir Malevich Str., 03150, Kiev, Ukraine. E-mail: office@paton.kiev.ua

Heat-resistant polymers are ever wider applied in aerospace, automotive and other industries. For the process of thermopastics welding it is important to study temperature distribution inside the overlap welded joint. In this work thermal and deformation processes in welding with embedded element of sheet samples from high-tech heat-resistant polymer ZEDEX ZX-410 based on polyetherimide, were modeled. Melting temperature and polymer material destruction temperature were the criteria for optimization of process parameters. Good correlation is shown for modeling results and experimental data obtained both from thermal studies of the process of welded joints formation, and mechanical testing of the formed welded joints. 9 Ref., 12 Figures.

Keywords: *welding with embedded element, high-tech polymers, modeling, testing*

With advance of engineering and technology new polymers with improved service properties are being developed in the world, which oust metals and other traditional materials in many spheres. High-tech heat-resistant polymers of polyarylene class — polyetherimide (PEI), polyetherketone (PEEK), polyphenylsulphide (PPS) and others have been actively used over the recent years. These polymers are thermoplastics, so that various welding processes are used for joining them. Application of high-tech heat-resistant polymers is the most intensively developing in aerospace and automotive industries, as well as in mechanical engineering, where it is often necessary to make extended welds of a complex geometry and in difficult-of-access places. Such joints are usually welded using an embedded heating element.

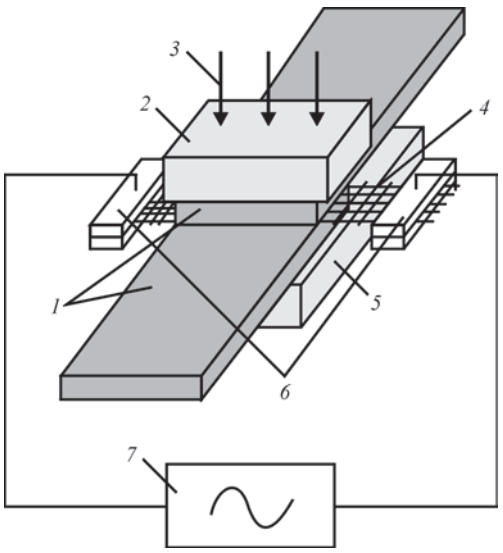

Figure 1. Schematic of the process of welding with embedded element: *1* — samples; *2* — clamp; *3* — working pressure; *4* — embedded element; *5* — base; *6* — electric contacts; *7* — power source

Typical schematic of the process of welding with embedded element is given in Figure 1. The embedded element is made from metal wire, mesh or strip and when applied it becomes the source of thermal energy, and after welding it remains inside the welded joint. Heating of the embedded element is most often performed due to heat evolution at passing of electric current through it, supplied from a special power source. Working pressure is applied to the joint outer surface to ensure sound weld formation.

Polymer material melting and joint formation in welding with embedded element occur in a closed space between the surfaces of the parts being welded. The possibility of monitoring the heating and cooling of the butt is limited, welding process parameters are usually set and regulated by indirect indices (embedded element heating rate, amount of formed flash, etc.). The main problem in welding with embedded element is ensuring an optimum amount of heat, which evolves in the welding zone. In welding extended welds of a complex shape, there is high probability of appearance of unheated zones and formation of lacks-of-penetration in some sections of the

*K.O. Zvorykin, NTUU «I. Sikorsky KPI» took part in performance of the work.

joint, and as well as appearance of overheated zones with destructured polymer material in other sections. Therefore, preliminary mathematical modeling of thermomechanical processes in welding with embedded element to determine the admissible parameters of embedded elements in heating parts of different geometry is urgent.

Beginning of application of welding with embedded elements for joining parts from high-tech polymers was accompanied by appearance of the first mathematical models of the process of embedded element heating [1]. These are two-dimensional models developed for assessment of temperature distribution during welding over the surface of strip embedded elements made from metal or PEEK-based carbon fibre composite.

Furtheron, 3D thermal models of the process of welding with embedded element were developed, which already allowed for thermal conductivity of polymer material, heat losses and latent heat. Difficulties of modeling the contact surfaces between the embedded element and the parts being welded were noted, which were described on the basis of physical concept of thermal conductivity of the gap. Known are three-dimensional models of thermal processes in welding with embedded element of PEEK- and PEI-based polymer composite materials with preliminary preparation of the embedded element by covering it with film from the main polymer material [2].

Similar work was performed for cases of welding PEEK- and PEI-based multilayer glass-fibre composites using metal mesh [3, 4]. Models of dynamic distribution of temperature over the embedded element surface were used for determination of admissible and critical parameters of the welding process. The criteria for parameter optimization were physical characteristics of matrix polymer, namely temperature of melting and destruction, and modeling adequacy was compared with experimental data. Mathematical modeling results were used to determine the regions («windows») of optimum values of the main parameters of thermistor welding (specific power and heating duration) for embedded elements from metal mesh of different typesizes [5].

Ukraine is one of the few countries in the world with its own aerospace industry. However, investigations on welding of high-tech polymer materials using embedded element have not been performed here up to now. In this study, domestic experimental work and modeling of the process of welding with embedded element of PEI-based heat-resistant polymer material ZX-410 of ZEDEX trade mark were conducted for the first time. Unlike foreign studies [1, 3], in this work the influence of thermal energy released by the embedded element during welding on the extent of residual plastic deformation was additionally determined and potential zones of the start of welded joint fracture were predicted, when modeling the process of thermistor welding. In the experimental part of the work, the main thermophysical parameters of the used polymer material and their behaviour, depending on temperature, were studied. The obtained data were further used as a basis for model development. To assess the adequacy of modeling the thermal processes, a series of experiments was performed on welding overlap joints with synchronous measurement of temperature in several points directly inside the welded joint and recording the thermal fields by filming in infrared spectrum.

Experimental. *Materials.* Sheet polymer material ZX-410 based on high-tech heat-resistant PEI was used in the work. The main thermomechanical characteristics of this material at the temperature of 20 °C claimed by the manufacturer, are as follows: density ρ — 1.33 kg/dm^3; fracture strength σ_t — 101 MPa; relative elongation at fracture δ — 25 %; Young's modulus E — 3368 MPa; maximum working temperature T_{max} — 180 °C; vitrification temperature T_{gl} — 210 °C; melting temperature T_m — 320 °C; coefficient of thermal expansion α — $4.0 \cdot 10^{-5}$ 1/K (at up to 0 °C temperature) and $5.8 \cdot 10^{-5}$ 1/K (at 0–50 °C temperature); coefficient of thermal conductivity λ — 0.25 W/(m·K); coefficient of heat capacity c_p — 1.85 kJ/(kg/K).

At modeling thermal processes it is important to take into account the considerable dependence of the coefficient of thermal conductivity λ and coefficient of heat capacity c_p of polymer material on temperature values. Temperature dependencies of thermophysical coefficients of ZX-410 material were determined experimentally.

Coefficient of thermal conductivity λ at different temperatures was determined using an all-purpose dynamic calorimeter IT-400, in which measurements are performed with monotonic linear temperature rise. In order to take measurements, samples were made from the studied material in the form of discs of 15 mm diameter and 1.2 mm height, which were conditioned for a 24 h day at the temperature of 22 °C directly before taking the measurements. Because of the technical limitations of the instrument, λ coefficient was measured in the temperature range of 22–250 °C every 5 °C.

Derived temperature dependence of λ is given in Figure 2. One can see that an initial abrupt lowering of the coefficient of thermal conductivity with temperature rise, and subsequent stabilization of its values are observed. When the temperature of 100 °C has been reached, monotonic growth of λ coefficient begins right up to the temperature of material vitrification (approximately 217 °C [6]), where extremum

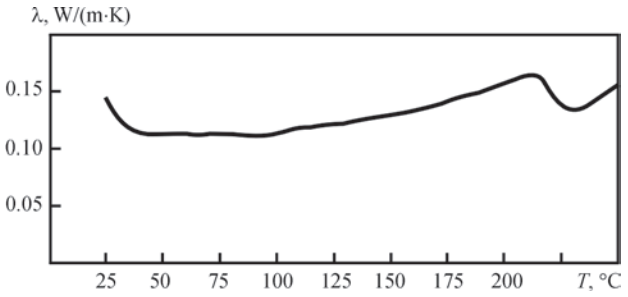

Figure 2. Dependence of the coefficient of thermal conductivity λ of polymer material ZX-410 on temperature

of the graph, lowering and subsequent increase of λ values are observed.

Temperature dependence of the coefficient of thermal conductivity c_p of ZX-410 material was studied by the method of differential scanning calorimetry (DSC) [7] in DSC Q2000 instrument of TA Instruments Company (USA) in inert atmosphere of higher purity gaseous nitrogen. Measurements were conducted in the temperature range of 40–450 °C at a constant heating rate of 20 °C/min. Before taking measurements, samples of 10 mg weight were conditioned for a 24 h day at the temperature of 22 °C and weighed in electronic scales ANG50C with the accuracy of 0.0001 g.

Derived temperature dependence of the coefficient of heat capacity is given in Figure 3. Two peaks appear on the curve at T = 220 and 326 °C. The peak at T = 220 °C is attributed to such a thermal process as devitrification of PEI amorphous phase, and at T = = 326 °C it is attributed to melting of its crystalline phase. Measured value of vetrification temperature practically coincides with the value derived at determination of the coefficient of thermal conductivity (Figure 2). At devitrification, a local maximum of the coefficient of heat capacity forms, which in this case is associated with enthalpy restoration [8], when the polymer density rises, and its free volume is reduced [9]. The process of the crystalline phase melting with energy ΔH = 96 J/g is of a two-stage nature. The premelting process in the temperature range

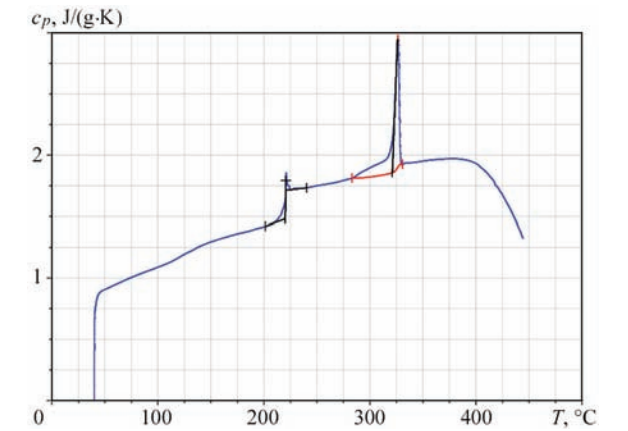

Figure 3. Dependence of the coefficient of heat capacity c_p of polymer material ZX-410 on temperature

of 280–320 °C is indicative of presence of a certain interphase connection and crystallites of a complex structure in the polymer.

Experimental setup for welding with embedded element. Experimental set up was assembled in keeping with the schematic given in Figure 1. Sheet samples of ZX-410 polymer material of 25×100 mm size of thickness from 8 mm were welded with an overlap. The embedded element used was metal woven mesh from high-alloyed 12Kh18N9T steel, manufactured in keeping with the requirements of GOST 3826 and having the following parameters: wire diameter of 0.25 mm, pass-through cell size of 0.8 mm, material specific resistance of 0.7–0.8 Ohm·mm²/m. Embedded element dimensions were 25×60 mm, those of the welded joint were 25×25 mm. Power was supplied from a source of alternating current of 50 Hz mains frequency with adjustable ranges of voltage of 1–50 V and current of 5–45 A. Working pressure in welding was 0.2 MPa.

Temperature measurement. Temperature measurement during welding with embedded element was performed in three characteristic points inside the welded joint (Figure 4). Point *1* is designed for measurement of embedded element temperature and it is located in immediate vicinity of its longitudinal wire. Point *2* is located in the mesh cell center, and point *3* is in the polymer above the embedded element.

TKhK thermocouples (type *L*, 0.5 mm diameter) were used for temperature measurement. Fixation and recording of signals of three thermocouples were performed using OVEN UKT-38 multichannel instrument connected to a computer. Temperature field of visible surfaces of the welded joint was also recorded using DT-918 infrared imager.

Mechanical testing. In the world practice, ASTM D1002-10 standard developed for adhesive joints is usually used for mechanical testing of overlap joints of sheet polymer materials, in view of the absence of a special standard. In keeping with it, lap shear strength (LSS) is determined for welded joints. A similar GOST 14759 was also developed for determination of adhesive joint strength.

In this work, mechanical tensile testing of overlap welds was conducted in keeping with the require-

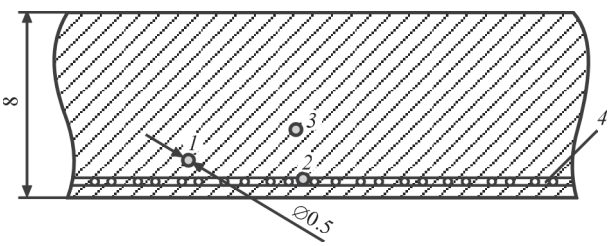

Figure 4. Temperature measurement points during welding with embedded element (*1–3*) — longitudinal wires of embedded element mesh

ments of the above standards in rupture machine FP-10 (Germany) with the speed of mobile clamp movement of 25 mm/min. Both complete welded joints and samples cut out of them in the form of longitudinal strips were tested.

Mathematical model. Different kinds of software, such as COMSOL Multiphysics, ANSYS and Abaqus FEA can be used for modeling thermomechanical problems of heat distribution, development of strains and stresses. Abaqus FEA was used in this work. Abaqus software package was initially oriented to solution of the most complex and important problems, allowing for all kinds of non-linearity, as well as performance of multidisciplinary static and dynamic analysis within one algorithm. Such a concept positively distinguishes Abaqus from other programs of this level (ANSYS software package uses third-party program LS-DYNA for analysis of strongly nonlinear and fast processes). It allows using Abaqus to solve multipurpose tasks within a common approach, combining the advantages of explicit and implicit FEA procedures and their combination.

When plotting the model, the embedded heating element from woven metal mesh was simplifiedly modeled as a homogeneous and isotropic metal strip. Embedded element heating, when electric current was passed through it, was modeled as volume heat evolution, equivalent to applied electric power. The criterion for parameters optimization was melting temperature and destruction temperature of ZX-410 polymer material. A two-dimensional model of the joint was used, which is given in Figure 5. Dimensions of welded samples were equal to 8×25×50 mm, with working pressure of 0.2 MPa. In keeping with experimental data, heating time was equal to 100 s.

Calculations were performed using Abacus/Standard submodule — one of the two main solvers of Abaqus software package, using the implicit formulation of finite element method, which is described below.

The following conditions were taken as boundary ones: a limitation was applied to the base of sample *2* (Figure 5), which prevented its displacement in the direction of *X* and *Y* axes, as well as rotation around *Z* axis; surface heat flow was applied to sample edges, which characterized heat removal into the ambient medium (coefficient of thermal conductivity of air).

Results and their discussion. Process of welding with embedded element proceeded in the stationary mode, without molten metal displacement. Heat transfer from the heating embedded element occurs mainly due to thermal conductivity of polymer material. Therefore, in the used two-dimensional model solution of the stationary equation of heat conductivity was performed by finite element method. Here, experimentally derived temperature dependencies of thermophysical coefficients of the studied material were used (Figures 2, 3).

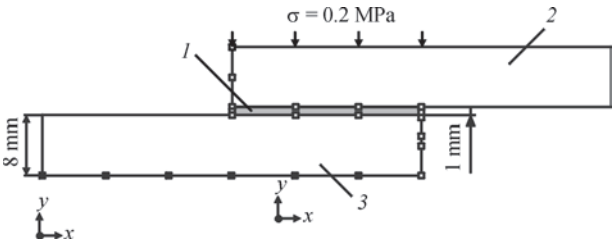

Figure 5. Schematic of a two-dimensional model of overlap joint in welding with embedded element: *1* — embedded element; *2* — sample *1*; *3* — sample *2*

Heat distribution from the heating element into the polymer matrix follows the Fourier thermal conductivity law:

$$q = -kA\frac{\partial T}{\partial x}, \quad (1)$$

where q is the heat flow; A is the area over which the heat flow is distributed; k is the material thermal conductivity; $\partial T/\partial x$ is the temperature gradient in the heat flow direction.

Determinant equation of equilibrium for finite element model has the following form:

$$P^N - I^N = M^{NM}\ddot{u}^M, \quad (2)$$

where P^N is the vector of external force; I^N is the vector of internal force; $M^{NM}\ddot{u}M$ is the vector of the force of inertia of the material.

Internal forces are determined by equations given below:

$$I^N = \int_V \beta^N / \sigma V, \quad (3)$$

where V is the model volume; $\sigma(x)$ are the stresses in point x; $\beta^N(x)$ is the extent of deformation — displacement, which is determined in interpolation assumptions in element $\dot{\varepsilon} = \beta^N \dot{u}^n$.

Dynamic equilibrium suggests that the forces of d'Alembert are considerable:

$$M_{NM}\ddot{u}^M, \quad (4)$$

where M^{NM} is the mass matrix; $\ddot{u}^M$ is the vector of acceleration.

Static equilibrium means that the forces of d'Alembert change slowly, are constant in time, and $M^{NM}\ddot{u}^M \approx 0$.

Abaqus/Standard uses the Newton method for static equilibrium solution. It is assumed that this is a supposed solution at iteration i, $u^N_{(i)}$, so that the Taylor series will have the following form:

$$P^N - I^N + \left(\frac{\partial P^N}{\partial u^M} - \frac{\partial I^N}{\partial u^M}\right)c^M + ... = 0, \quad (5)$$

which can be written as

$$P^N - I^N = K^{NM}c^M, \quad (6)$$

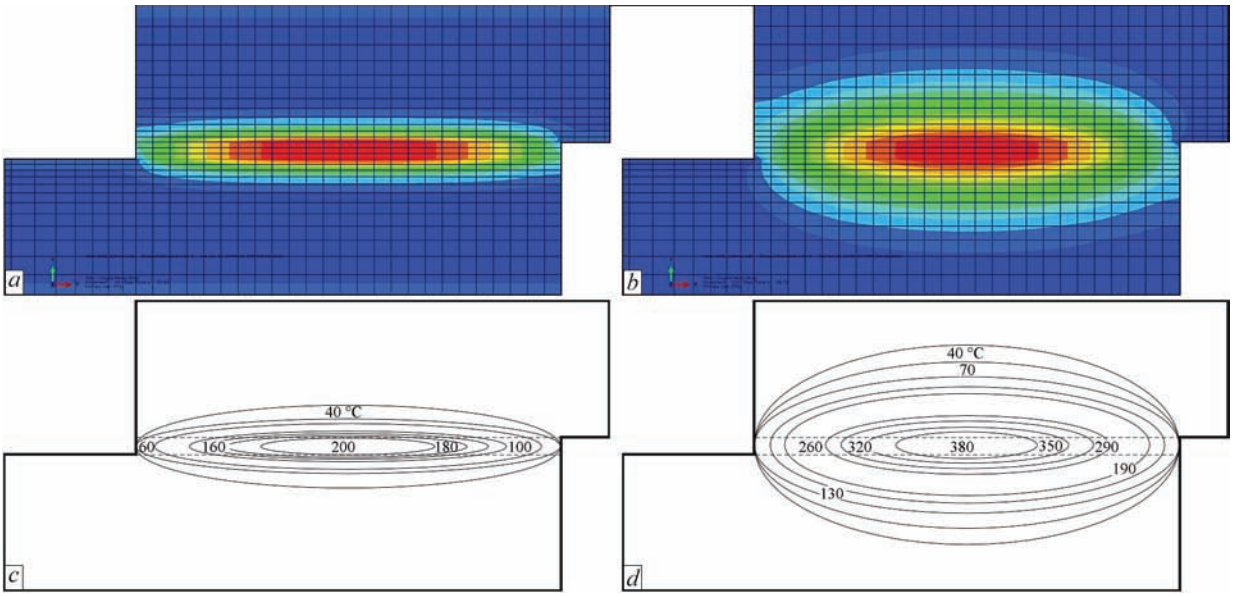

Figure 6. Temperature field at the initial (*a*) and final (*b*) moments of time of the welding process and their isotherms (*c*, *d*), respectively

where $K^{NM} = \frac{\partial I^N}{\partial u^M} - \frac{\partial P^N}{\partial u^M}$ is the system rigidity, or Jacobian matrix; c^M is the correction to the solution of degrees of freedom N.

Increment Δu is corrected according to equation

$$\Delta u^N_{(i+1)} = \Delta u^N_{(i)} + c^N_{(i)}, \quad (7)$$

Iterations are repeated at each increment until convergence has been reached, which means that:

- contact conditions are satisfied in each point;
- equilibrium has been reached in each point;
- equilibrium of moments has been reached in each point.

Exact implementation of the Newton method includes non-symmetrical Jacobian matrix, as it is shown in the presented matrix of connected equations:

$$\begin{pmatrix} K_{uu} & K_{u\theta} \\ K_{u\theta} & K_{\theta\theta} \end{pmatrix} \begin{Bmatrix} \Delta u \\ \Delta\theta \end{Bmatrix} = \begin{Bmatrix} R_u \\ R_\theta \end{Bmatrix}, \quad (8)$$

where Δu, $\Delta\theta$ are the corrections for incremental movement and temperature; K_{ij} are the submatrices of bound Jacobian matrix; R_u and R_θ are the mechanical and thermal nullity vector, respectively.

Main equation of heat transfer in the matrix form can be written as

$$[C]\{\dot{T}\} + [K]\{T\} = \{Q\}, \quad (9)$$

where $[C]$ is the matrix of specific heat; $\{\dot{T}\}$ is the time derivative of temperature; $[K]$ is the matrix of effective thermal conductivity; $\{T\}$ is the vector of nodal temperatures; $\{Q\}$ is the vector of effective heat flow in the node.

For stationary thermal analysis, when temperature is independent on time, equation of heat transfer is simplified to the following form:

$$[K]\{T\} = \{Q\}. \quad (10)$$

It should be noted that solution of thermal conductivity equation was performed sequentially in different moments of time. At the initial stage of heating

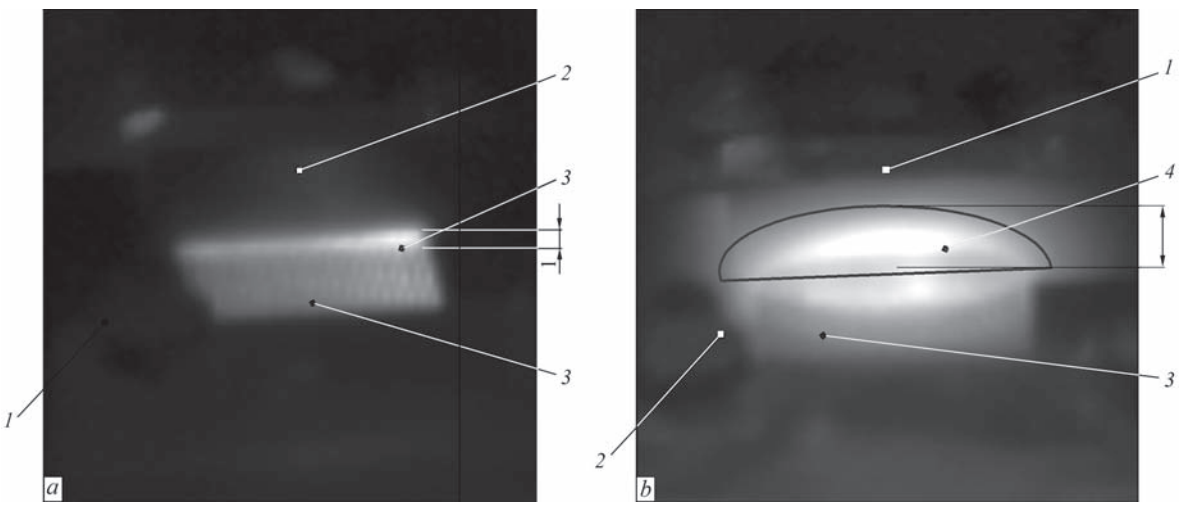

Figure 7. Successive illustrations of the process of welding with embedded element: *a* — 12 s (T_{max} = 160 °C); *b* — 100 s (T_{max} > > 400 °C); *1* — sample *2*; *2* — sample *1*; *3* — flash; *4* — embedded element

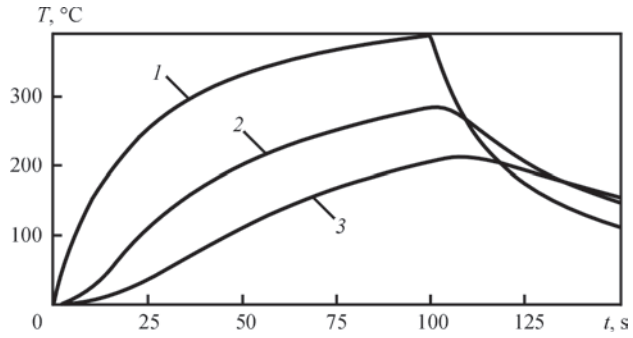

Figure 8. Results of modeling temperature variation in characteristic points of the welded joints: *1* — temperature on embedded element surface; *2* — temperature at 0.5 mm distance from embedded element surface; *3* — temperature in polymer layers removed from embedded element plane

the temperature is rather uniformly distributed by the width of the heating element (Figure 6, *a*, *c*). Non-uniformity of temperature distribution is increased by the end of the process of welded joint heating (Figure 6, *b*, *c*), the central regions being heated more. This is associated with more intensive heat removal along the embedded element edges. After completion of the process of weld cooling, the overall temperature level in the welding zone is reduced. However, the temperature field takes a spherical shape with a maximum in the center.

To check the adequacy of the results obtained at modeling of thermal processes, successive recording of the change of the temperature field of welded joint side surface during welding was performed in infrared range using a thermal imager. One can see in infrared photos that with the start of the welding process (Figure 7, *a*) the free zone of the embedded element is predominantly heated with gradual surface melting of the polymer material at the joint edge. Futheron, with heating of the embedded element, the temperature maximum is concentrated in the welded joint central part that corresponds to the data obtained in mathematical modeling. Under the impact of pressing force, flash forms in this part of the welded joint. At the final stage of heating and after cooling (Figure 7, *b*) the thermal field takes an ellipsoidal shape with a maximum in the center. Obtained experimental data demonstrate the thermal field on the side surface of the welded joint that is why they differ somewhat from the data of the proposed calculation model, which considers the thermal field inside the welded joint.

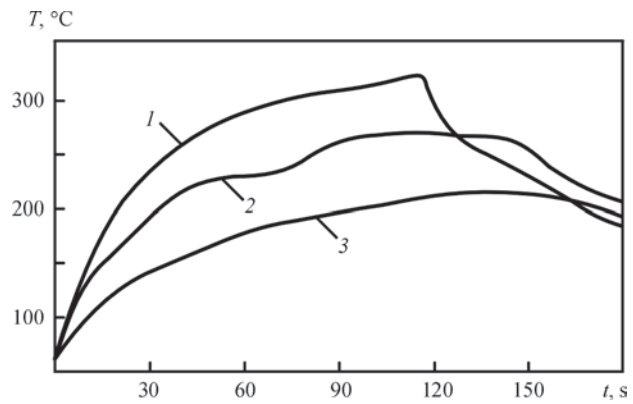

Figure 9. Results of experimental variation of temperature in characteristic points of the welded joint (for description of *1–3* see Figure 8)

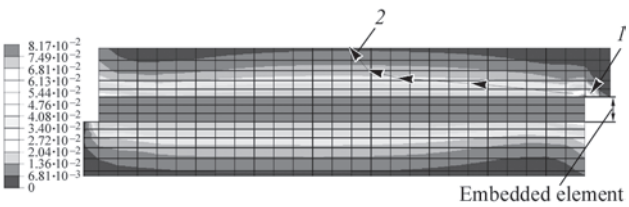

Figure 10. Field of equivalent plastic deformations in overlap welded joint: *1* — zone with maximum value of residual plastic deformation; *2* — fracture path

Modeling results were used to plot the graphs of temperature variation (Figure 8) during welding with embedded element — mesh in characteristic points of the welded joint, shown in Figure 4.

Graphs derived experimentally at direct measurement of temperature with thermocouples during welding with embedded element at heating duration of 120 s, are given in Figure 9. It should be also noted that despite the difference in the duration of the heating process, the graphs are analogous and are of a similar shape that confirms the effectiveness of modeling and similarity of thermal processes running in the welded joint under different welding conditions.

Both in the calculation and experimental graphs, polymer material temperature in the mesh plane (point *2*) rises gradually as heat propagates from heated longitudinal wires of the mesh from both sides towards the center. As during modeling a simplified representation of the heater in the form of a homogeneous and isotropic metal strip was used instead of the mesh, model graph of point *2* corresponds to 0.5 mm distance from the heater surface. Therefore, experimental temperature in this point is somewhat higher, compared to the data obtained during modeling.

Temperature in polymer layers removed from embedded element plane (point *3*) rises slowly, compared to polymer matrix adjacent to the embedded element that is attributable to low thermal conductiv-

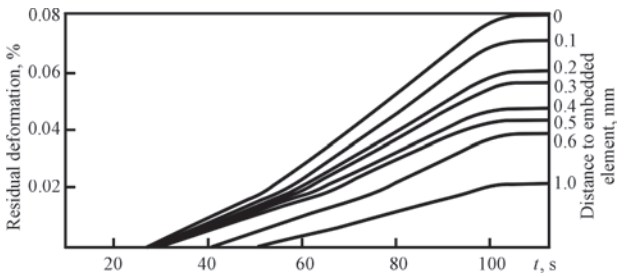

Figure 11. Change of the magnitude of plastic deformation of the polymer in time at different distances from embedded element surface

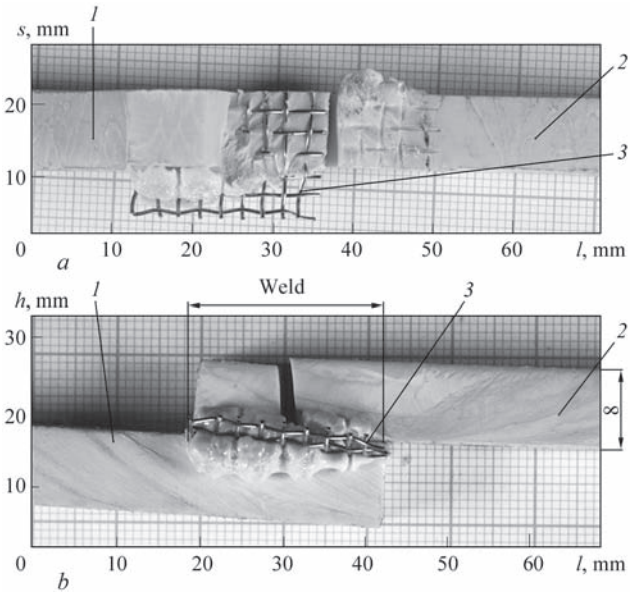

Figure 12. Nature of fracture of a sample (*l* — length, *h* — height; *s* — width), cut out of equivalent overlap joint of ZX-410 polymer material: *a* — top view; *b* — side view (*1* — sample *2*; *2* — sample *1*; *3* — embedded element)

ity of the material. Material melting point is achieved here practically at the moment of switching the power source off. However, because of the inertia of heat propagation process, material heating in this zone goes on for some more time. This promotes more uniform molten state of the base material and further normal formation of the welded joint. The curve of temperature change in point *3* derived as a result of modeling, confirms the obtained experimental results.

Modeling of residual plastic deformations, due to heat evolution during welding, was also performed in this work. Modeling results are shown in Figure 10.

At the initial heating stage plastic deformation is practically absent, its development is recorded only on welded joint edges, where the embedded element contacts the base polymer material. Further on plastic deformations uniformly propagate along the embedded element plane. The nature of variation of the magnitude of plastic deformation in time at different distances from the embedded element is given in Figure 11. One can see that the largest values of plastic deformation are achieved at the welded joint edge (Figure 10, pos. 1).

Mechanical testing of overlap welded joints, produced in optimum modes, shows that their strength is equivalent to that of the base material (Figure 12, *a*), where fracture ran not through the welded joint but through the base material. Fracture of overlap joint at shear testing (Figure 12) occurs along a trajectory, similar to the line of largest values of plastic deformation, derived at modeling (Figure 10, *d*).

Conclusions

The work presents a two-dimensional model of development of temperature fields in welding with embedded element of sheet polymer material ZX-410, allowing for its temperature-dependent thermophysical parameters, which also allows for development of residual plastic deformations at heating in the welding zone. Modeling correctness is confirmed by experimental temperature measurements during welding using thermocouples and thermal imager. It is shown that sample fracture at shearing load starts in the region of the greatest plastic deformations and propagates in the direction towards the weld central region.

Thus, proceeding from the results of modeling it allows to prediction of possible regions with higher risk of lack-of-penetration formation along the embedded element edges that is associated with non-uniform temperature distribution in the welding zone. Such lacks-of-penetration should be compensated by the respective increase of overlap weld area.

The developed models can be later used for prediction of optimum heating modes in welding with embedded element, in our case — metal mesh.

1. Jakobsen, T.B., Don, R.C., Gillespie, Jr. J.W. (1989) Two-dimensional thermal analysis of resistance welded thermoplastic composites. *Polymer Eng. and Sci*., 29(**23**), 1722–1729.
2. Ageorges, C., Ye, L., Mai, Y.-W. et al. (1998) Characteristics of resistance welding of lap shear coupons. Pt 1. Heat transfer. *Composites Part A*, **29**, 899–909.
3. Colac, Z.S., Sonmez, F.O., Kalenderoglu, V. (2002) Process modeling and optimization of resistance welding for thermoplastic composites. *J. of Composite Materials*, 36(**6**), 721–744.
4. Yousefpour, A., Simard, M., Octeau, M.-A. et al. (2005) Process optimization of resistance-welded thermoplastic composites using metal mesh heating elements. In: *Proc. of SAMPE* (USA, Long Beach).
5. Stavrov, D., Nino, G.F., Bersee, H.E.N. et al. (2007) Optimization tool for welding of thermoplastic composites. In: *Proc. of 16th Int. Conf. on Composite Materials* (Japan, Kyoto, Fellow Doshisha University).
6. Ibeh, C.C. (2011) *Thermoplastic materials: Properties, manufacturing methods and applications.* CRC Press, Boca Raton, Fl.
7. Menczel, J.D., Prime, R.B. (2009) *Thermal analysis of polymers: Fundamentals and applications*. John Wiley & Sons, Inc., Hoboken, New Jersey, USA.
8. Simon, S.L. (1997) Enthalpy recovery of poly(ether imide): Experiment and model calculations incorporating thermal gradients. *Macromolecules*, 30(**14**), 4056–4063.
9. (2007) *Principles and applications of thermal analysis*. Ed. by P. Gabbott. Wiley, Blackwell Publishing Ltd.

Received 24.07.2017